Understanding salinity evolution in the Moroccan Ghiss-Nekor aquifer using differential mapping technique

Abdelhak Bourjila[1,*], *Fouad* Dimane[1], *Lahcen* Benaabidate[2], *Mohammad* Ghalit[3], *Morad* Taher[4], *Salim* Kamari[5], *Yahya* El Hammoudani[1], *Iliass* Achoukhi[1], and *Khadija* Haboubi[1]

[1]Laboratory of Engineering Sciences and Applications (LSIA)- Materials Science, Energy and Environment (SM2E) Research team, ENSAH / Abdelmalek Essaâdi University, Al Hoceima, Morocco
[2]Department of Environment, Laboratory of Functional Ecology and Environment Engineering, Faculty of Sciences and Techniques, University Sidi Mohamed Ben Abdellah, Fez, Morocco
[3]Laboratory of Research and Development in Engineering Sciences, Faculty of Sciences and Techniques of Al-Hoceima (FSTH), Abdelmalek Essaâdi University, Tetouan, Morocco
[4]Department of Geology, Applied Geosciences and Geological Engineering Research Team, FSTH, Abdelmalek Essaâdi University, Al Hoceima, Morocco
[5]Environmental Management and Civil Engineering Research Team, Laboratory of Applied Sciences, ENSAH, Abdelmalek Essaâdi University, Al Hoceima, Morocco

Abstract. Assessing spatiotemporal groundwater hydrochemistry evolution is crucial for sustainable aquifer management. The Ghiss-Nekor aquifer, located in a semi-arid coastal region, requires a comprehensive grasp of hydrochemical shifts for proactive degradation mitigation. Accordingly, the differential mapping technique (DMT) has been employed to assess the salinity evolution in the study area. In 2015 and 2022, 48 and 52 groundwater samples were respectively analyzed. As a result, an overall increase in salinity was observed within the Ghiss-Nekor aquifer, particularly near the shoreline, where in some areas the TDS variations (ΔTDS) exceeded +7000 mg/L. ΔCl^- reached up to +129 meq/L near the coast. Similarly, ΔNa^+, ΔSO_4^{2-}, ΔMg^{2+}, ΔCa^{2+}, ΔK^+, and ΔHCO_3^-, showed values up to +94 meq/L, +22 meq/L, +17 meq/L, +10 meq/L, +1 meq/L, and +5 meq/L, respectively, along the coast. In contrast, a decline in the levels of these ions was noted across most of the plain, especially in the southern portion. Positive major ions levels near the sea indicate ongoing freshwater degradation due to seawater intrusion. DMT approach showed its effectiveness in assessing the spatiotemporal changes occurring within aquifers. These findings advocate for broader DMT application in safeguarding aquifers impacted by salinization, promoting sustainable development.

1 Introduction

Seawater intrusion (SWI) is a natural or anthropogenic phenomenon in which seawater increases the salinity of groundwater (fresh or brackish) in a coastal aquifer system. SWI into coastal aquifers can have significant repercussions, such as degrading groundwater quality and reducing available freshwater resources [1]. Increased groundwater salinity can make it unsuitable for human consumption and agricultural use, and can also lead to the disruption of groundwater-dependent ecosystems [2].

Disturbances in the water cycle can affect available water supplies, which can have an impact on economic activities, such as agriculture, and the drinking water needs of local populations. In short, monitoring salinity levels in groundwater is crucial to protect natural ecosystems and the human activities that depend on them.

Additionally, the implementation of sustainable groundwater management is essential to prevent a global water crisis, with a particular focus on developing countries such as Morocco [3].

The Ghiss-Nekor coastal aquifer, spanning Al Hoceima and Driouch provinces, is a vital water source along Morocco's Mediterranean coast. Prolonged droughts, common in semi-arid areas, have led to insufficient fresh surface water for the population. This has led to a significant dependence on groundwater and seawater desalination. However, ongoing droughts and extensive groundwater extraction, particularly during the high-population summer seasons, are expected to exacerbate seawater intrusion and other salinization-inducing processes, such as evapotranspiration. This will consequently elevate the salinity levels in the Ghiss-Nekor aquifer, further compromising its water quality.

* Corresponding author: abourjila@uae.ac.ma

The assessment of salinity evolution is essential for ensuring the sustainable management of aquifers. However, the application of certain techniques in assessing aquifer salinization imposes significant prerequisites, necessitating either a profound comprehension of statistical methodologies, exemplified by the utilization of Multivariate Statistical Analysis (MVSA) [4], or a proficient command of Geographical Information System (GIS) tools, as exemplified by mapping the outcome of Hydrochemical Facies Evolution Diagrams (HFE-D) [5,6]. This prerequisite constitutes a notable limitation in the widespread adoption of these methodologies. Alternatively, techniques that are more straightforward may be employed, such as direct interpretation of descriptive statistics or comparative analysis of hydrochemical data distribution maps. However, these latter methods may prove inadequate in detecting subtle changes within specific hydrogeological contexts [5,7].

In light of this, the current study underscores a method for examining spatiotemporal variations in aquifer salinization that is both straightforward and highly effective. Termed the Differential Mapping Technique (DMT), this approach leverages GIS software to detect alterations in specific areas over two separate time intervals. This is typically achieved through the comparison of raster maps of a particular geographic area generated at different temporal intervals. While the DMT finds extensive application across various disciplines for detecting and mapping changes in land use/land cover [8], vegetation [9], soil erosion [10], and other physical landscape attributes, its application in monitoring salinity evolution remains relatively unexplored. Notable exceptions include studies conducted by [7] and [5].

Hence, the main objective of the current study is to highlight the significance of DMT in evaluating the spatiotemporal evolution of salinity, using the Ghiss-Nekor alluvial aquifer as a case study. The outcomes of this research are intended to furnish an efficient methodology for monitoring groundwater salinity over time, ultimately enabling improved aquifer management strategies.

2 Study area

Ghiss-Nekor plain is a coastal area extending approximately 14 kilometers along the shoreline. It is located southeast of Al Hoceima city, positioned within 35°5' N and 35°13' N latitudes, and 3°45' W and 3°54' W longitudes (Figure 1). The plain exhibits an average slope of around 1% from south to north and covers an area of approximately 100 square kilometers.

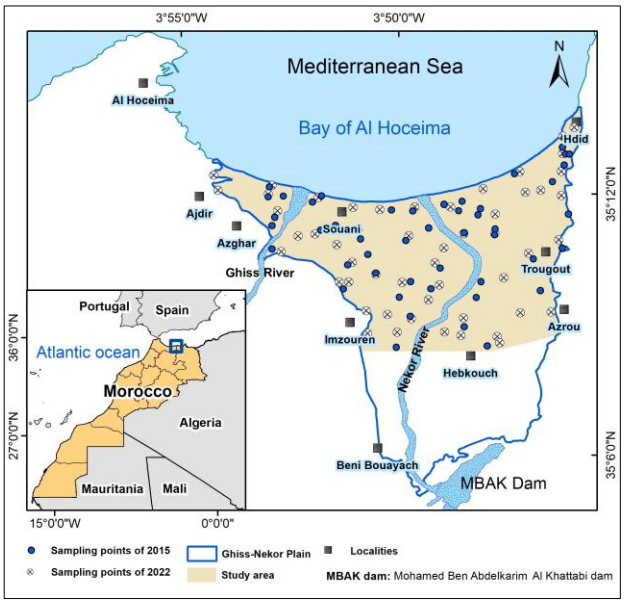

Fig. 1. Geographical location of the Ghiss-Nekor plain.

In terms of its geographical shape, the Ghiss-Nekor plain takes on a triangular form and is intersected by two principal intermittent rivers. The Ghiss river traverses the northwestern section, while the Nekor river runs through the central part. Beneath the plain lies the Ghiss-Nekor aquifer, widely recognized as the most significant alluvial aquifer in the Moroccan Mediterranean region. It currently supplies the majority of the drinking water to the city of Al Hoceima and surrounding urban centers. This is attributed to the limited storage capacity of the MBAK dam, a result of the siltation phenomenon [11]. This aquifer, along with the surface water reserves, primarily receives its supply from the Nekor and Ghiss basins. The predominant lithologies in the two basins consist mainly of shale, limestone, and marly flysch.

3 Materials and methods

3.1 Groundwater sampling and analysis

In May 2015, data from 48 wells were gathered as reported in the study by Chafouq et al. [12]. Subsequently, in January 2022, a total of 52 water samples were acquired from both drilled wells and boreholes located within a coastal area spanning approximately 64 km², situated no more than 8 km from the coast.

In order to maintain consistency in methodology and uphold data integrity, the collection, storage, transportation, and laboratory analysis of the groundwater samples adhered to the criteria specified in "Water Analysis (9th edition)" [13]. The chemical parameters under examination in this study encompassed total dissolved solids (TDS), along with concentrations of major ions: sodium (Na^+), potassium (K^+), magnesium (Mg^{2+}), calcium (Ca^{2+}), bicarbonates (HCO_3^-), nitrates (NO_3^-), chlorides (Cl^-), sulfates (SO_4^{2-}). The analysis of various parameters was conducted using the measuring equipment and techniques outlined in **Table 1**.

Table 1. Measurement instruments and methods for groundwater chemical parameters.

Parameters	Measuring instruments and methods
TDS	Determined through the application of the formula TDS = Σ cations + Σ anions
Na^+, K^+	Flame photometer (Model: ELICO CL 378) (accuracy ± 0.5 ppm)
Ca^{2+}, Mg^{2+}	Titration with EDTA
Cl^-	Titration with silver nitrate (0.1 N)
HCO_3^-	Titration with hydrochloric acid (0.1 N)
NO_3^-, NO_2^-, NH_4^+, PO_4^{3-}, and SO_4^{2-}	The colorimetric determination method using a UV-VIS Spectrophotometer (LANGE HACH DR-6000) (precision ± 1 nm)

While the sampling periods of 2015 and 2022 aligned with different seasons, both intervals experienced similar climatic conditions, characterized by high temperatures and low precipitation rates. This highlights the significance of ensuring comparable climatic conditions during the two sampling periods, even when the selected seasons differ.

3.2 GIS-based analysis

In the groundwater sector, the predominant mapping techniques are inverse distance weighting (IDW) and kriging interpolations. Recent research studies [14–16] consistently affirm that the IDW method surpasses the kriging tool in terms of accuracy. Additionally, the IDW approach is esteemed for its user-friendly nature, rapidity, and precision of results, as noted by many authors [17], [18], and [19]. Consequently, the spatial interpolation of major ion concentrations for both the 2015 and 2022 sampling periods was executed using the IDW technique integrated into ArcGIS. In this method, the weight assigned to each point is determined by the reciprocal of the distance, and the interpolated value of the sampling point is computed using the following equation:

$$Z = \frac{\sum_{i=1}^{N} \frac{1}{D_i^q} \times Z_i}{\sum_{i=1}^{N} \frac{1}{D_i^q}} \quad (1)$$

Zi represents the value of the neighboring sampling point *i* (i = 1, 2, …, N); *Di* signifies the distance between the interpolated point and the neighboring sampling point; *q* is a constant, typically set to a value of 2 [20].

By employing the differential mapping technique (DMT), we generated maps showing the spatiotemporal variation of major ions for the two sampling campaigns. The Raster calculator, an integral part of Map Algebra within ArcGIS, was the GIS tool utilized to create these maps. This tool is recognized for its simplicity and robustness, allowing the execution of various Spatial Analyst tools, operators, and functions for comprehensive geographic analysis [21,22].

A simple method involves employing map algebra through local operations on a cell-by-cell basis. To perform the DMT, the subtraction operation was used to subtract two superimposed rasters. The first raster highlights the geographical distribution map of the studied ion measured in 2022 campaign, while the second raster depicts the geographical distribution map of the same ion measured in 2015 campaign, where the raster cells denote the concentration of the analyzed ion. Through the application of this method, the concentration difference for each cell was obtained. The resulting map indicates both positive (+) and negative (-) values, with + values denoting an increase in ion levels and - values indicating a drop in concentrations. Each major ion underwent this process, as outlined in equation (2), resulting in a distinct map for each ion.

$$\Delta C_i\ map = C_i\ map_{2022} - C_i\ map_{2015} \quad (2)$$

Where $\Delta C_i\ map$ is the generated map for the studied major ion, $C_i\ map_{2022}$ is the map showing the distribution of ion concentration for the 2022 campaign, while $C_i\ map_{2015}$ is the map showing the distribution of ion concentration for the 2015 campaign.

4 Results and discussion

The hydrochemical analysis of the major ions generally indicates an increase in maximum concentration values between 2015 and 2022. For instance, the maximum TDS level surged significantly from 6768 mg/L to 10015 mg/L. Similar trends were observed for Na^+ and Cl^- maxima, which rose from 65.60 meq/L to 111.30 meq/L, and from 85.04 meq/L to 146.9 meq/L, respectively (**Table 2**). The elevated concentrations of major ions near the coast can be primarily attributed to seawater intrusion [5,23], while in the rest of the Ghiss-Nekor plain, the phenomenon is explained by the lithological nature of the basins intersected by the two main rivers, Ghiss and Nekor. These basins are predominantly composed of shale, limestone, and marly flysch [24,25]. These statistical data are insufficient to determine which zones are affected by this increase in salinity, which led us to propose the DMT as a technique for spatiotemporal assessment of salinization in the Ghiss-Nekor alluvial aquifer.

Table 2. Maximum and minimum concentrations of major ions in the two sampling periods.

		May 2015		January 2022	
Parameter		Min	Max	Min	Max
TDS	mg/L	1549	6768	1449	10015
Ca^{2+}	meq/L	5.72	18.37	2.97	20.76
Mg^{2+}		2.24	30.19	4.72	32.96
Na^+		8.88	65.60	5.96	111.3
K^+		<DL*	2.30	0.04	1.04
HCO_3^-		4.80	11.52	2.50	11.70
SO_4^{2-}		7.87	45.41	4.90	33.17
Cl^-		7.92	85.04	4.46	146.9
NO_3^-		0.12	1.99	0.00	1.99

*DL: Detection limit

The spatiotemporal variation maps (refer to figure 2), generated through DMT, showed notable patterns associated with the exacerbation of salinization. The temporal differences of TDS (ΔTDS) (see figure 2a) displayed a

noteworthy surge in salinity in regions proximate to the sea. Noteworthy spikes, ΔTDS surpassing +7000 mg/L in some instances, were particularly evident along the eastern bank of the Nekor river and in close proximity to the Ghiss river mouth. The remainder of the plain exhibited either a minor increase (indicated by yellow and green colors in the ΔTDS map) or a decrease in salinity, reaching a ΔTDS as low as -2613.68 mg/L.

The examination of the chloride anions variation (ΔCl^-) (Figure 2b) shows a rise of up to +129 meq/L in the coastal region to the east of the Nekor river and around the mouth of the Ghiss river. Likewise, ΔNa^+, ΔSO_4^{2-}, ΔMg^{2+}, ΔCa^{2+}, ΔK^+, and ΔHCO_3^- show elevated levels near the coastline, reaching +94 meq/L, +17 meq/L, +22 meq/L, +10 meq/L, +1 meq/L, and +5 meq/L respectively (figure 2c to *i*). Conversely, a decrease in ion concentrations is noted in most of the Ghiss-Nekor plain, especially in the southern part.

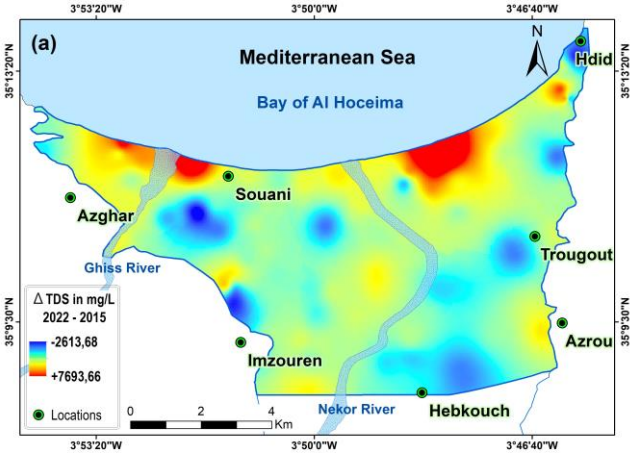

Fig. 2. Spatial and temporal variations of major ions in the Ghiss-Nekor aquifer (2015 and 2022): **(a)** ΔTDS, **(b)** ΔCl^-, **(c)** ΔNa^+, **(d)** ΔSO_4^{2-}, **(e)** ΔMg^{2+}, **(f)** ΔCa^{2+}, **(g)** ΔK^+, **(h)** ΔHCO_3^-, and **(i)** ΔNO_3^-. (-) values indicate a rise in ion level, whereas (+) values indicate a decline in ion level.

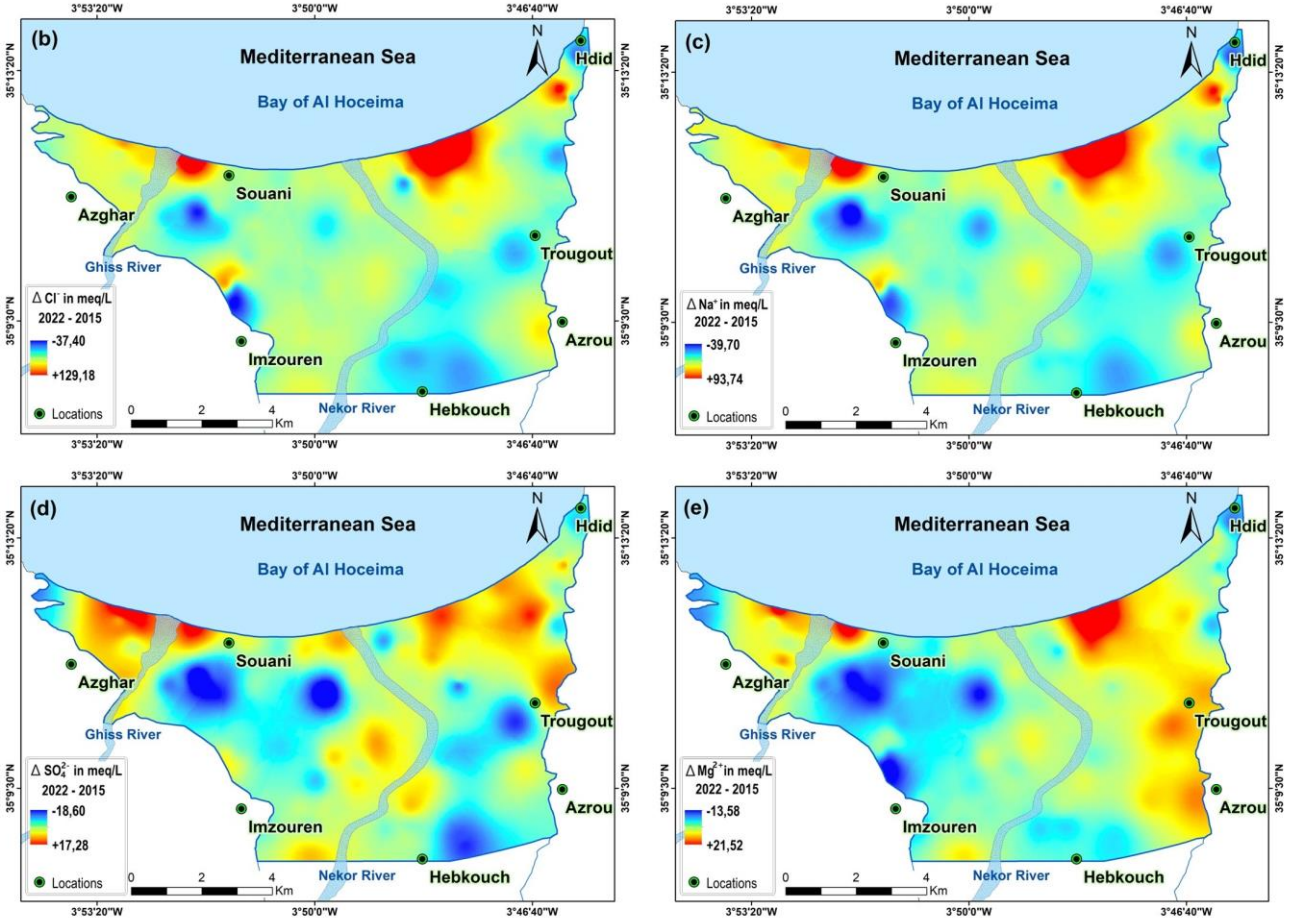

Fig. 2. (Continued)

The elevated salinity levels near the coast suggest that it is primarily attributed to seawater intrusion (SWI). This conclusion is supported by the findings of SWI assessment studies conducted by authors [23] and [5], which utilized multivariate statistical analysis, ionic ratios, HFE-Diagrams, and their corresponding maps. In addition to highlighting the occurrence and extent of SWI, as previously assessed in our study area by authors [26 - 31], and [12], DMT also reveals the progression of salinization linked to various geogenic and anthropogenic factors, including SWI.

As for ΔNO_3^-, it is notably elevated in the far northeast of the study area, near Imzouren city, and in Azrou, where values can reach up to +1.49 meq/L. The increase in nitrate levels near the Imzouren city may be attributed to wastewater infiltration into the aquifer due to the high population density in this area (figure 3) [32]. On the other hand, the rise in ΔNO_3^- in other areas, characterized by low population density, could be linked to agricultural fertilizer usage [23].

In summary, the maps clearly demonstrate a significant increase in major ion concentrations from 2015 to 2022, particularly in areas close to the sea. This confirms a worsening trend of seawater intrusion in the Ghiss-Nekor coastal aquifer over time. The study effectively tracks the evolution of salinization in this aquifer between the two years under examination.

While the inclusion of hydrochemical data from years between 2015 and 2022 would undoubtedly enhance the precision of tracking salinization evolution in the Ghiss-Nekor aquifer, these results are already highly promising, providing a straightforward method to assess the progression of environmentally detrimental phenomena like salinization. Such an approach could significantly aid decision-making in water management, particularly in regions where aquifers face threats not only from salinization but also from other pollutants carried by infiltrating water. Therefore, it is strongly recommended to continue employing the technique in future studies dedicated on monitoring salinization, not only in the Ghiss-Nekor coastal aquifer but also in various regions across the globe.

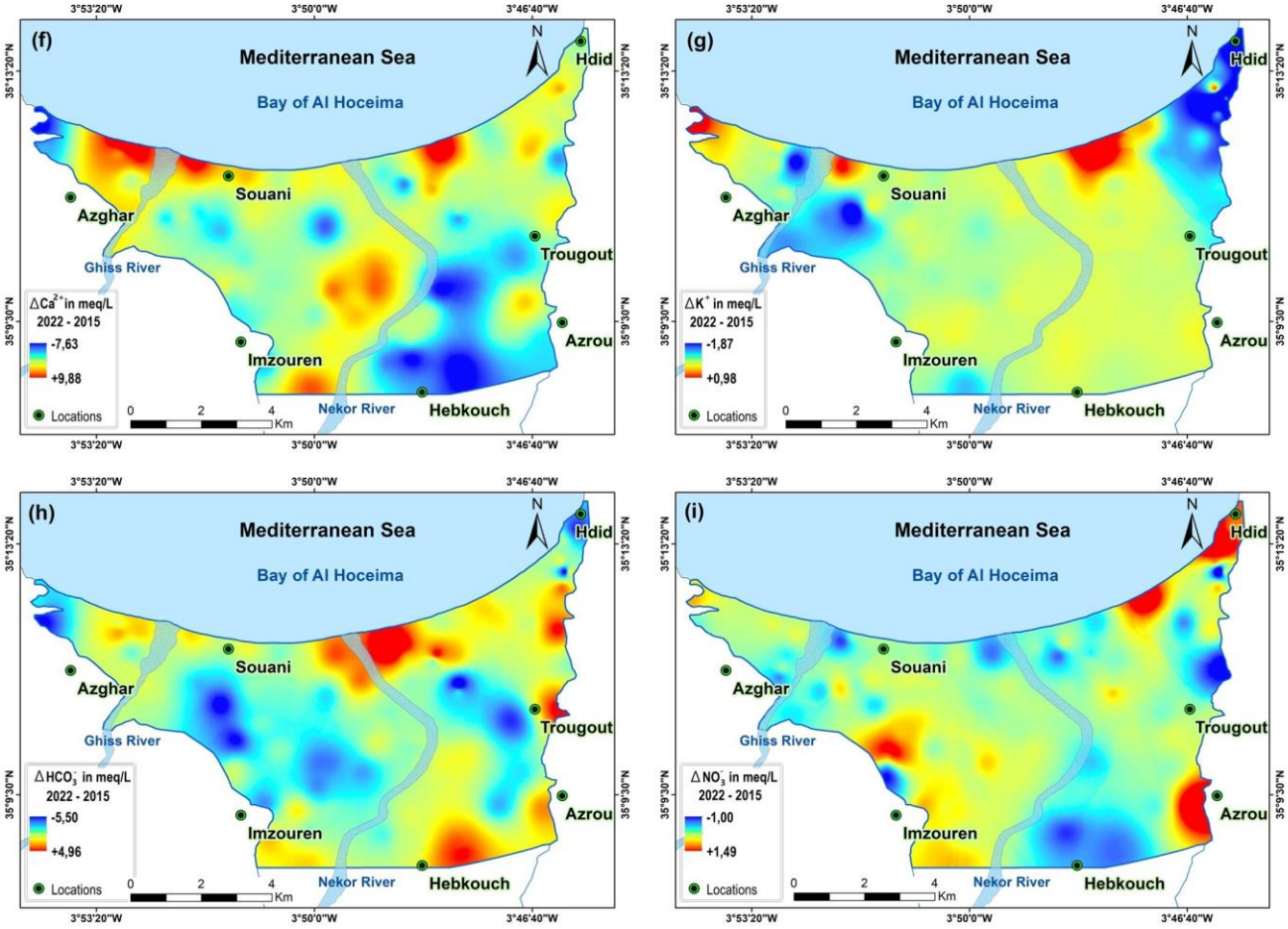

Fig. 2. (Continued)

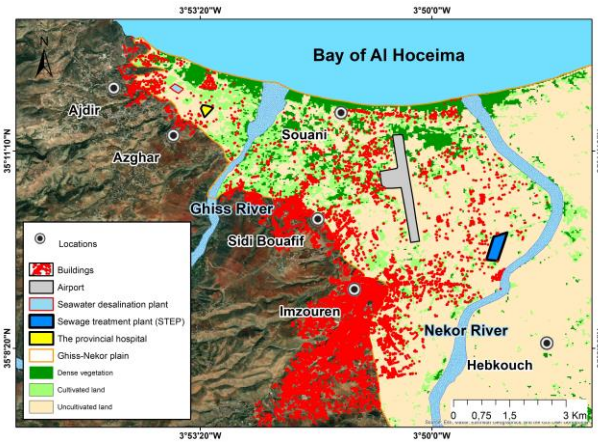

Fig. 3. LULC in the western part of the Ghiss-Nekor plain.

5 Conclusion

The study aims to highlight the importance of the Differential Mapping Technique (DMT) in monitoring the evolution of salinization in the coastal aquifer of Ghiss-Nekor. The results demonstrate a worsening of salinization in the study area between 2015 and 2022, particularly near the coast, strongly indicating the advancement of seawater intrusion. These findings vividly illustrate how DMT can offer a straightforward solution to complex issues like aquifer salinization. This study provides a clear application of this promising technique in the fields of hydrogeology and hydrochemistry, strongly advocating for its continued use in future studies aimed at evaluating the evolution of salinization or other types of groundwater pollutants. Furthermore, despite the limitation stemming from a lack

of data over an extended period, the study has the potential to provide valuable information for decision-makers responsible for groundwater management in the study area. This knowledge can be instrumental in formulating effective strategies to mitigate the impacts of salinization and ensure the long-term sustainability of the aquifer system.

We want to extend our heartfelt thanks to the reviewers for their invaluable feedback and constructive criticism, which enhanced the quality of this article. I also extend special thanks to Imad El Barkani for his insightful advice during the writing process. Additionally, I am indebted to Abdellah El Omrani and Mohamed Ettoukouki for their indispensable assistance during the fieldwork, significantly enhancing the quality and depth of the study. Their collective contributions have played a crucial role in shaping this work.

References

1. A. Lassiter, Current Opinion in Environmental Sustainability **50**, 208 (2021).
2. M. Soumaia, D. Lotfi, L. Yann, S. Gerhard, H. Mohamed, and M. Rajouene, Journal of African Earth Sciences **147**, 443 (2018).
3. M. Taher, T. Mourabit, I. Etebaai, H. C. Dekkaki, N. Amarjouf, A. Amine, B. Abdelhak, A. Errahmouni, and S. Azzouzi, Geomatics and Environmental Engineering **17**, 83 (2023).
4. A. Parisi, M. R. Alfio, G. Balacco, C. Güler, and M. D. Fidelibus, Science of The Total Environment **862**, 160697 (2023).
5. A. Bourjila, F. Dimane, M. Ghalit, M. Taher, S. Kamari, Y. El Hammoudani, I. Achoukhi, and K. Haboubi, Water Cycle **4**, 104 (2023).
6. E. Giménez-Forcada, Journal of Hydrology **517**, 617 (2014).
7. T. Slama and A. Sebei, Journal of African Earth Sciences **170**, 103915 (2020).
8. M. Asuquo Enoh, R. Ebere Njoku, and U. Chinenye Okeke, Advances in Space Research (2022).
9. A. Nasser Mohamed Eid, C. O. Olatubara, T. A. Ewemoje, H. Farouk, and M. T. El-Hennawy, International Soil and Water Conservation Research **8**, 66 (2020).
10. C. Hudson and P. J. Soar, Environmental Research **219**, 115050 (2023).
11. M. Taher, T. Mourabit, A. Bourjila, O. Saadi, A. Errahmouni, F. E. Marzkioui, and M. E. Mousaoui, Geomatics and Environmental Engineering **16**, 95 (2022).
12. D. Chafouq, A. El Mandour, M. Elgettafi, M. Himi, I. Chouikri, and A. Casas, Journal of African Earth Sciences **139**, 1 (2018).
13. J. Rodier, B. Legube, N. Merlet, and R. Brunet, *L'analyse de l'eau - 9ème édition - Eaux naturelles, eaux résiduaires, eau de mer: Eaux naturelles, eaux résiduaires, eau de mer*, 9e édition (Dunod, Paris, 2009).
14. S. Hajji, N. Allouche, S. Bouri, A. M. Aljuaid, and W. Hachicha, International Journal of Environmental Research and Public Health **19**, 155 (2022).
15. W. Yang, Y. Zhao, D. Wang, H. Wu, A. Lin, and L. He, Int J Environ Res Public Health **17**, E2942 (2020).
16. R. B. Zolekar, R. S. Todmal, V. S. Bhagat, S. A. Bhailume, M. S. Korade, and S. Das, Environ Dev Sustain **23**, 4433 (2021).
17. J. Hu, in *1995 ESRI User Conference Proceedings* (1995).
18. N. U. Kura, M. F. Ramli, S. Ibrahim, W. N. A. Sulaiman, and A. Z. Aris, Environmental Science and Pollution Research **21**, 7047 (2014).
19. K. Rina, P. S. Datta, C. K. Singh, and S. Mukherjee, Current Science 335 (2013).
20. P. Rao, Y. Wang, Y. Liu, X. Wang, Y. Hou, S. Pan, F. Wang, and D. Zhu, Journal of Hydrology: Regional Studies **43**, 101189 (2022).
21. ESRI, ArcGIS Desktop (2023).
22. T. Shirabe, Computers, Environment and Urban Systems **36**, 456 (2012).
23. A. Bourjila, F. Dimane, M. Ghalit, M. Taher, Kamari, I. Achoukhi, Y. EL Hammoudani, and O. Saadi, (2022).
24. G. O. Badmus, O. D. Akinyemi, A. M. Gbadebo, and J. A. Oyedepo, Heliyon **6**, e05661 (2020).
25. S. Benabdelouahab, A. Salhi, M. Himi, J. E. Stitou El Messari, and A. Casas Ponsati, Environmental Earth Sciences **78**, (2019).
26. D. Chafouq, E. Mandour, M. Elgettafi, M. Himi, S. Bengamra, Y. Lagfid, and A. Casas, in (2016).
27. A. Salhi, Géophysique, hydrogéologie et cartographie de la vulnérabilité et du risque de pollution de l'aquifère de Ghis-Nekor (Al Hoceima, Maroc), 2008.
28. N. Iouzzi, A. Larabi, and M. Faouzi, 6 (2011).
29. A. Khouakhi, S. Niazi, O. Raji, and A. N. E. Fahchouch, International Journal of Hydrology Science and Technology **5**, 133 (2015).
30. T. Kouz, H. Cherkaoui Dekkaki, S. Mansour, M. Hassani Zerrouk, and T. Mourabit, in *Groundwater and Global Change in the Western Mediterranean Area*, edited by M. L. Calvache, C. Duque, and D. Pulido-Velazquez (Springer International Publishing, 2018), pp. 169–177.
31. M. Ghalit, E. B. Yousfi, M. Zouhairi, E. K. Gharibi, and J.-D. Taupin, Moroccan Journal of Chemistry **5**, 5 (2017).
32. S. Kamari, H. E. Ouarghi, M. Ghalit, A. Makan, and A. Bourjila, Ecol. Eng. Environ. Technol. **24**, (2023).